# Meshless Modelling for Heat-based Robotic Navigation of Radio Frequency Catheter Ablation

K. A. Mountris[1], R. Schilling[2], A. Casals[3], and H. A. Wurdemann[1]

[1]*Mechanical Engineering Dept., University College London,*
[2]*Barts Heart Centre, St Bartholomew's Hospital,*
[3]*Research Center for Biomedical Engineering, Universitat Politecnica de Catalunya*
*k.mountris@ucl.ac.uk*

## INTRODUCTION

Radio frequency catheter ablation (RFCA) of cardiac arrhythmia is commonly performed by navigating the catheter manually. Nevertheless, remote navigation techniques where catheter steering is performed using either a magnetic field or robotically are available. Clinical experience with these techniques demonstrated that higher contact forces can be achieved with robotic compared to magnetic field navigation [1]. This translates into more effective ablation lesions, but if excessive contact force is applied it may lead to higher risk of cardiac perforation [2]. However, the robotic navigation system is no longer commercially available and advancements have been stalled. To ensure high effectiveness and low complication risk in next-gen robotic navigation systems, tissue heat distribution should be taken into account. Computational models for heat distribution simulation predict lesion formation effectively [3]. However, their clinical application is limited since they have been developed for single-site ablation and numerical accuracy depends on the quality of mesh discretization. In this work, we propose a novel meshless model to simulate tissue heat distribution during robotic navigation assisted ablation. The model accounts for non-zero initial conditions and time dependent boundary conditions to simulate multi-site ablation. The meshless Fragile Points Method (FPM) is employed for the numerical solution of the model to ensure its suitability for clinical application, since FPM does not require the definition of a mesh [4], [5].

## MATERIALS AND METHODS

In FPM, a domain of interest ($\Omega$) is represented by a set of randomly distributed points which are enclosed in non-overlapping subdomains that partition $\Omega$. Local discontinuous polynomials are used as trial functions. For a subdomain $E_0$ enclosing the point $P_0$, the trial function $u_h$ is given by:

$$u_h(\boldsymbol{x}) = u_0 + (\boldsymbol{x} - \boldsymbol{x}_0) \cdot \nabla u\Big|_{P_0}, \quad \boldsymbol{x} \in E_0 \tag{1}$$

where $u_0$ is the value of $u_h$ at $P_0$ and $\boldsymbol{x}_0$ the coordinates vector of $P_0$. $\nabla u\Big|_{P_0}$ is estimated in terms of $u_h$ values at neighbor points of $P_0$ using Generalized Finite Differences [6]. Tissue heat distribution is then modelled by solving the bioheat Pennes equation:

$$\rho c(T)\frac{\partial T}{\partial t} - \nabla \cdot (k(T)\nabla T) = q \text{ in } \Omega \tag{2}$$

where $\rho$ is density, $c(T)$ specific heat, $t$ time, $k(T)$ thermal conductivity, $T$ temperature. The heat source $q = \sigma(T)|\nabla\Phi|^2$ is produced by the RF current and is obtained by solving the electrical potential equation:

$$\nabla \cdot (\sigma(T)\nabla\Phi) = 0 \text{ in } \Omega \tag{3}$$

where $\sigma(T)$ is electrical conductivity and $\Phi$ electrical potential. Multi-site ablation is modelled using the temperature field from previously ablated sites as initial condition in Equation (2). Time-dependent Dirichlet conditions are employed in Equation (3) to account for the time interval between the start and end of the different ablations. Given the ablation starting time ($t_s$) at a given site, the time-dependent Dirichlet conditions are expressed as:

$$\Phi = \Phi_D u(t - t_s) \text{ in } \Gamma_D \tag{4}$$

where $\Gamma_D$ is the Dirichlet boundary and $u(t - t_s)$ the step function:

$$u(t - t_s) = \begin{cases} 1 & \text{if } t \geq t_s \\ 0 & \text{if } t < t_s \end{cases} \tag{5}$$

An ablation protocol with two ablation sites s1, s2 of a 3D porcine ventricular tissue block with dimensions $40 \times 40 \times 20$ mm was considered. Density $\rho = 1076$ kgm$^{-3}$, initial specific heat $c_0 = 3017$ Jkg$^{-1}$K, initial thermal conductivity $k_0 = 0.518$ Wm$^{-1}$K, and initial electrical conductivity $\sigma_0 = 0.54$ Sm$^{-1}$ were used. Ablation sites were located at the top tissue surface at s1 $= (0, -1, 20)$ mm and s2 $= (0, 1, 20)$ mm. Ablation time was $t_a = 30$ s. Temperature $T = 37°$C was imposed as boundary condition. The surface of the catheter was held at $T = 22°$C. Electrical potential at the bottom tissue surface was set $\Phi = 0$V and $\Phi = 20$V at the surface of the catheter. Simulations were performed with catheter indentation at perpendicular position and rotated around the x-axis by a 30° angle. To distinguish between the

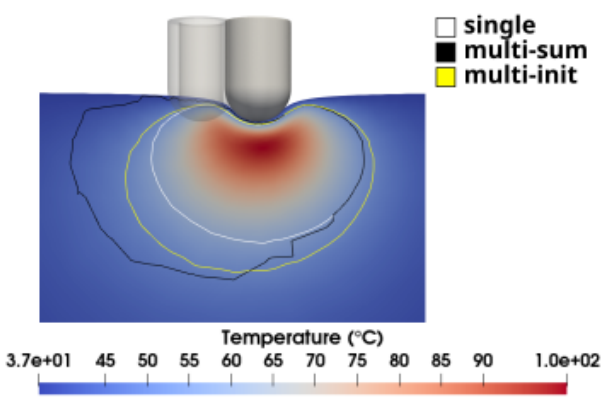


**Fig. 1** $T \geq 50°$C isolines for single and multi-site ablation for perpendicular catheter indentation ($R_1 = 0°$, $R_2 = 0°$). The lesion in single ablation (white) is underestimated compared to multi-site with initial condition (yellow).

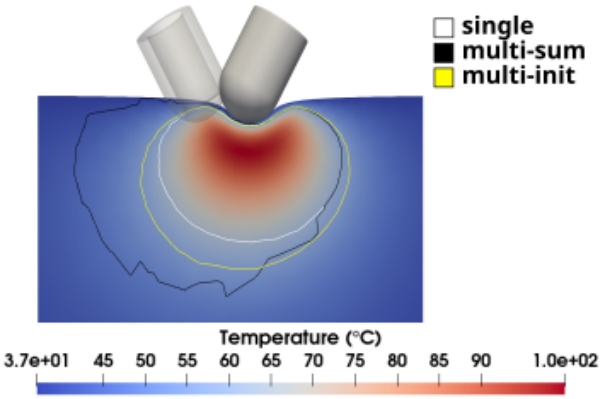


**Fig. 2** $T \geq 50°$C isolines for single and multi-site ablation for indentation with angles $R_1 = 30°$, $R_2 = -30°$. Lesion underestimation in single-site ablation is observed.

different simulations we used the abbreviation $R_x = a°$, where $x$ denotes the ablation site and $a°$ the catheter rotation angle. For instance, $R_{s1} = 0°$, $R_{s2} = 0°$ denotes the simulation where the catheter was perpendicularly indented at both sites. Similarly, $R_{s1} = 30°$, $R_{s2} = -30°$ denotes the simulation where the catheter was indented at an angle of 30° around x-axis at s1 and −30° around x-axis at s2. Indentation force was $F = 20$g in all simulations.

## RESULTS

The ablation lesion at site s2 from single-site ablation simulation was compared with the lesion obtained from the proposed multi-site ablation simulation (multi-init). A comparison with summed single-site heat maps (multi-sum) was also performed. The region receiving $T \geq 50°$C was considered as lesion since tissue heat damage is permanent above 50°C. Lesion width (W), depth (D), and maximum temperature ($T_{max}$) were computed to compare the heat maps obtained from the single, multi-init, and multi-sum simulations. Three different catheter rotation angles at s1, s2 were considered during simulations. These were namely ($R_{s1} = 0°$, $R_{s2} = 0°$), ($R_{s1} = 30°$, $R_{s2} = 30°$), and ($R_{s1} = 30°$, $R_{s2} = -30°$). Differences in the lesion characteristics between single and multi-init were up to 17.6% for W, 24.4% for D, and 6.1% for $T_{max}$ for ($R_{s1} = 0°$, $R_{s2} = 0°$) simulation. Similar results were demonstrated in simulations with different rotation angles. In Figures 1, 2 $T \geq 50°$C isolines are given for simulations with catheter rotation angles $R_{s1} = 0°$, $R_{s2} = 0°$ and $R_{s1} = 30°$, $R_{s2} = -30°$, respectively.

## DISCUSSION

In this study, a novel meshless FPM computational model was proposed to simulate multi-site ablation for next-gen robotic navigation systems. Multi-site ablation simulation was performed using the temperature distribution from previous ablations as initial condition. Lesion characteristics were evaluated for single-site and multi-site simulations. It was found that lesion characteristics were underestimated in single-site simulation. As shown in Figures 1 and 2, multi-init simulations predicted larger lesion compared to single-site simulations. While max temperature difference was in the range 5.7% - 6.1%, the lesion width was larger in multi-init heat maps by a range of 14.5% - 17.6%. and depth was larger in the range of 22.0% - 24.4%. Therefore, multi-site ablation simulation may assist in the formation of transmural lesions at lower tissue temperatures. The capacity of the presented computational model for meshless simulation of multi-site ablation has the potential to improve next-gen robotic navigation systems. Predicting heat maps while taking into account the heat accumulation from previous ablations could guide the robotic navigation system to deliver heat homogeneously to the area under treatment. Furthermore, since transmural lesions may be obtained for lower temperatures, the cardiac perforation risk due to excessive contact force could be reduced. Finally, since the proposed computational model is meshless it does not require a preprocessing step making its application in clinical robotic navigation systems straightforward.

## REFERENCES

[1] D. Steven, T. Rostock, H. Servatius *et al.*, "Robotic versus conventional ablation for common-type atrial flutter: a prospective randomized trial to evaluate the effectiveness of remote catheter navigation," *Heart Rhythm*, vol. 5, 2008.

[2] R. Bai, L. Di Biase, M. Valderrabano *et al.*, "Worldwide experience with the robotic navigation system in catheter ablation of atrial fibrillation: methodology, efficacy and safety," *Journal of cardiovascular electrophysiology*, vol. 23, 2012.

[3] A. Petras, M. Leoni, J. M. Guerra *et al.*, "A computational model of open-irrigated radiofrequency catheter ablation accounting for mechanical properties of the cardiac tissue," *International journal for numerical methods in biomedical engineering*, vol. 35, 2019.

[4] L. Dong, T. Yang, K. Wang, and S. N. Atluri, "A new fragile points method (fpm) in computational mechanics, based on the concepts of point stiffnesses and numerical flux corrections," *Engineering Analysis with Boundary Elements*, vol. 107, 2019.

[5] K. A. Mountris, L. Dong, Y. Guan *et al.*, "A meshless fragile points method for the solution of the monodomain model for cardiac electrophysiology simulation," *Journal of Computational Science*, vol. 65, 2022.

[6] T. Liszka and J. Orkisz, "The finite difference method at arbitrary irregular grids and its application in applied mechanics," *Computers & Structures*, vol. 11, 1980.